Available online at www.sciencedirect.com
SCIENCE DIRECT®
Journal of Crystal Growth 261 (2004) 520–525
JOURNAL OF CRYSTAL GROWTH
www.elsevier.com/locate/jcrysgro

Selective growth of ZnO nanorods on pre-coated ZnO buffer layer

Hsu-Cheng Hsu[a], Yung-Kuan Tseng[b], Hsin-Min Cheng[b], Jia-How Kuo[a], Wen-Feng Hsieh[a,*]

[a] *Institute of Electro-Optical Engineering, National Chiao Tung University, 1001 Tahsueh Rd., Hsinchu 30050, Taiwan*
[b] *Materials Reaserch Laboratories, Industrial Technology Reasearch Institute, 195 Section4 Chung Hsing Road, Chutung, Hsinchu 310, Taiwan*

Received 18 August 2003; accepted 24 September 2003
Communicated by M. Schieber

Abstract

Hexagonal ZnO nanorods have been selectively synthesized via vapor–solid process without gold catalysis on a pre-coated ZnO buffer layer. The presence of nanometer-sized pits or hills on the surface of ZnO buffer layer provides nucleation sites to which the zinc vapor is transferred and condensed. Followed by immediate oxidation the ZnO nanorods were grown on the buffer layer. Contrarily, the SEM images hardly show growth of irregular ZnO nanometer-sized products on the bare sapphire substrate. Besides a strong ultra-violet emission at 3.26 eV observed at room temperature, the coupling strength of the radiative transition to LO-phonon polarization field was deduced in use of the Huang–Rhys factor from low temperature photoluminescence spectra to show that single crystalline ZnO nanorods.

Keywords: A2. Growth from vapor; B1. Nanomaterials; B1. Zinc compounds; B2. Semiconducting II–VI materials

1. Introduction

One-dimensional (1D) semiconductor nanostructures, such as nanorods and nanowires, have become important fundamental building blocks for nanophotonic devices and offer substantial promise for integrated nanosystems [1,2]. Nanorods of various compound semiconductors including InP, GaAs, and GaP have recently synthesized in several research groups [3–5]. Much attention recently has been paid to the nano-structured materials such as ZnO and GaN which radiate ultraviolet (UV) emission. Especially, since ZnO has a wide bandgap of 3.37 eV at room temperature, high mechanical and thermal stabilities, and much larger free exciton binding energy (60 meV) than that of GaN (25 meV), it ensures an efficient excitonic emission up to room temperature. Recently, UV lasing for ZnO nanowires has been demonstrated by Huang et al. [6]. It is expected that a lower threshold optical pumping density

*Corresponding author. Tel.: +886-3-5745684; fax: +886-3-5716631.
E-mail addresses: hchsu.eo89g@nctu.edu.tw (H.-C. Hsu), wfhsieh@mail.nctu.edu.tw (W.-F. Hsieh).

0022-0248/$ - see front matter © 2003 Elsevier B.V. All rights reserved.
doi:10.1016/j.jcrysgro.2003.09.040

for lasing is due to the carrier confinement effect in 1D nanowires. Therefore, it has great potential applications for short wavelength photonic devices.

Various methods have been developed in synthesizing ZnO nanorods [7–13]. Previous effort in synthesis of high-quality ZnO rods had employed high-temperature process such as vapor–liquid–solid (VLS) mechanism, in which a metal liquid droplet acts as an active catalyst [14]. In this method, the growth temperature were maintained beyond 800°C and the nanorods were randomly grown on substrates. However, to establish an applicable process for the integrated photonic devices, one may have to develop a relatively low temperature and selective growth method for growing desired structures on the patterned templates. In this work, we demonstrated the possibility of the selective growth of ZnO nanorods on patterned ZnO buffer layer. The selectivity of ZnO naorods grown on low-temperature pulsed laser deposition (PLD)-film was significantly enhanced as compared with those directly grown on *c*-plane sapphire. The growth mechanism is discussed and the origin of the emission at low-temperature luminescence is also analyzed.

2. Experimental procedure

A high yield of ZnO nanorods were fabricated by the following procedure. The ZnO buffer layer was grown on *c*-plane sapphire by PLD technique at deposition temperature of 500°C in different oxygen pressure of 10^{-4}, 10^{-3} and 10^{-2} Torr. A ceramic ZnO target (99.99%) was ablated in a vacuum chamber using a KrF excimer laser with wavelength of 248 nm and pulse duration of 25 ns. A metal grid as a mask covered on part of the substrate was used to pattern the ZnO film. The preparation of ZnO nanorods was preceded by a low pressure chemical vapor deposition system (LP-CVD) with a quartz tube of 2 in in diameter, which was mounted inside a 120 cm long tube furnace. A powder mixture of pure ZnO powder (99.9%) and zinc metal powder (99.9%) was placed in an alumina boat as the starting materials. The boat was positioned in the center of the quartz tube and the substrate was placed 5 cm downstream from the mixed powder. After the system was evacuated to a pressure of less then 10 Torr by a mechanical pump, high-purity argon gas was introduced into the system with a flow rate of 30 sccm. Then the furnace temperature was increased to 500°C and maintained for 30 min while the experiment proceeded. After the system had been cooled to the ambient temperature, a gray-white colored product was found deposited on the substrate and the wall of the tube close to the low-temperature end of the furnace. The morphology and crystal structure of the products were characterized by atomic force microscope and field emission scanning electron microscope (FESEM; LEO 1530). The photoluminescence measurement was made using a 20 mW He-Cd laser at wavelength of 325 nm and the emission light was dispersed by a TRIAX-320 spectrometer and detected by a UV-sensitive photomultiplier tube. A closed cycle refrigerator was used to maintain the measurement temperature at 6 K.

3. Results and discussion

Fig. 1 displays the atomic force microscope topography of a ZnO buffer layer with the oxygen pressure of 10^{-2} Torr. It is seen that the film surface was non-uniform and with an average roughness of 1.3 nm. Presented in Fig. 2 is the SEM photograph of the nanorods grown on ZnO buffer layer with the oxygen pressure of 10^{-2} Torr. High yield of the nanorods were observed on ZnO buffer layer (left-hand side of the figure) but rare nanorods were observed on the other part of the sapphire substrate, where it was covered by the metal mask during the growth of ZnO buffer layer. The SEM-photograph shown in Fig. 3(a) is a magnified section of high yield ZnO nanorods, as can be seen, nanorods are well-defined hexagonal crystals with diameters of around 100–300 nm and lengths up to 3 μm. Fig. 3(b) shows the Energy-Dispersive X-ray (EDX) spectrum of this section, which indicates that the nanorods contain only Zn and O elements and notably no other elements are detected.

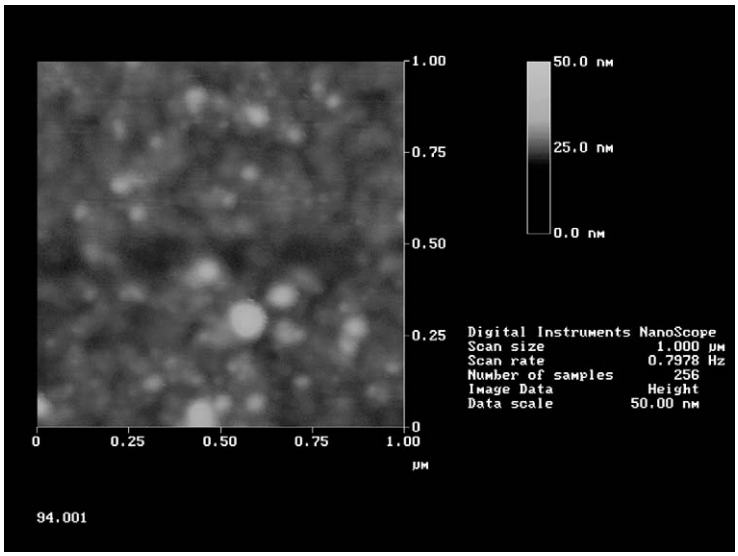

Fig. 1. AFM image showing the morphologies of ZnO buffer layer grown on a sapphire (0 0 0 1) substrate.

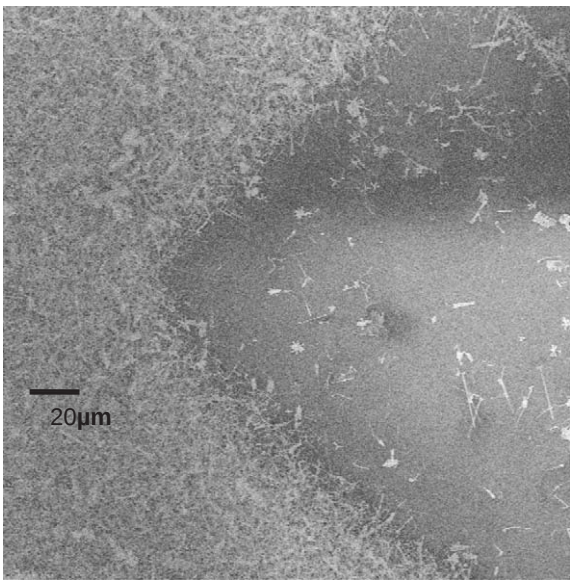

Fig. 2. SEM image of the ZnO nanorods showing two different positions.

The formation of ZnO nanorods includes two steps: nucleation and growth. For the conventional VLS process, metal catalyst such as gold is necessary to form the liquid metal–alloy droplets and the nanorods are grown through condensation of the source metal from the supersaturated liquid metal–alloy droplets followed by immediate oxidation. Since there are no metal catalysts involved in the growth process, no droplets were found at the ends of nanorods, which is the main feature of the VLS mechanism, the growth mechanism is not based on VLS but it is likely governed by vapor–solid process [15] or the so-called self-catalyzed VLS process [16]. As shown in AFM topography in Fig. 1, the presence of pits or hills with nanometer order on the surface of ZnO buffer layer may provide nuclear seeds for the thermally evaporized Zn atoms to condense onto the substrate [17]. Thus, the already condensed Zn not only acts as the seed but also provides an energetically favorite site for adsorption of oxygen.

It has been demonstrated that the morphology of the crystals is related to the relative growth rates of various crystal faces that bound the crystal; these growth rates are not only determined by the internal structure of the crystal but also affected by the growth conditions [18]. The SEM image in Fig. 2(a) indicates that the growth rates of the directions $\langle 0\,0\,1\rangle$, $\langle 1\,0\,1\rangle$, and $\langle 1\,0\,0\rangle$ of the ZnO crystal have the relationship of $R_{\langle 0\,0\,1\rangle} > R_{\langle 1\,0\,1\rangle} > R_{\langle 1\,0\,0\rangle}$. The anisotropic growth of the crystal causes formation of high aspect-ratio ZnO nanostructure and the ZnO

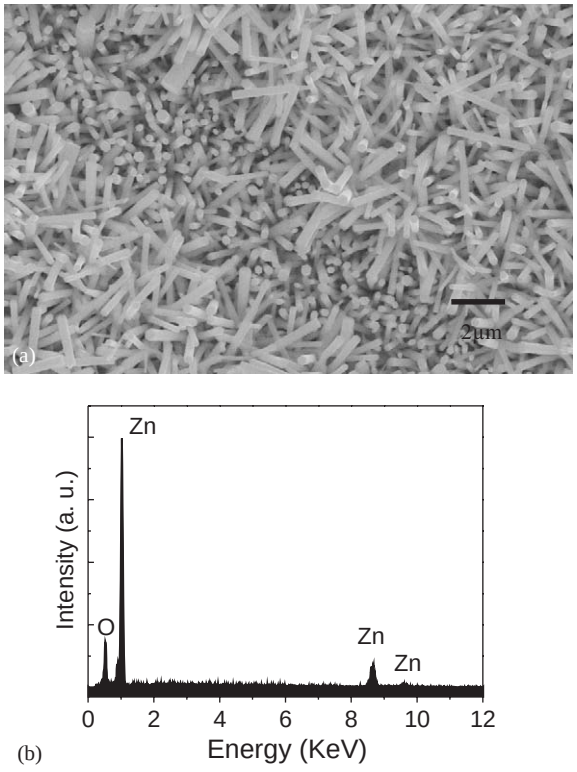

Fig. 3. (a) A typical high magnification SEM image to show shapes of ZnO nanorods and (b) EDX pattern of the ZnO nanorods.

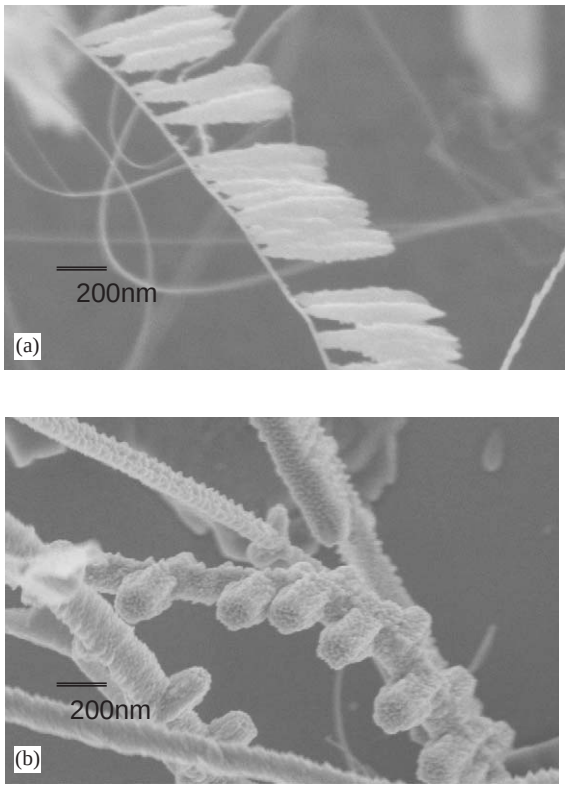

Fig. 4. 3D ZnO structures with several nanorods.

nanorods are preferentially oriented along the *c*-axis with prismatic morphology on their tops.

On the other hand, there are only very few nanorods on the bare sapphire. This is due to the smooth surface that may not serve as a nucleation site, Zn vapor is hardly condensed on the clear sapphire surface as compared with on the rough ZnO buffer layer. This result is consistent with the previous report on ZnO nanorods growth by MOVPE method [11] that a thin ZnO buffer grown at low temperature is a key factor for their growth method. Hence, according to the VS axial growth mechanism, pre-coated ZnO buffer layer is preferential to grow ZnO nanorods.

Fig. 4(a) and (b) displays an assembly of ZnO nano-homojunctions formed on several nanorods on the different morphology of buffer layer. If the surface of the nanorods is rough and the concentration of Zn reaches the critical vapor pressure, then the nano-branches will grow from the nano-valley on the surface of the nanorods. This growth mechanism of ZnO branch may be similar to the growth of self-catalyzed nanorods and is analogous to Jian's finding on SnO_2 nanodendrites [19]. They found the morphologies of the SnO_2 nanowires change under different oxygen gas flow. Unfortunately, we are still not able to completely control the growth conditions to obtain the desired types of ZnO branches.

The typical room temperature PL spectrum (see Fig. 4) of the ZnO nanorods shows besides a sharp emission located at 3.26 eV, which corresponds to the recombination of free exciton, another broad emission centered at 2.55 eV, which is attributed to excess Zn (or oxygen vacancy) or surface state emission. It is not surprising to observe free exciton emission at room temperature due to its large exciton binding energy (60 meV) as

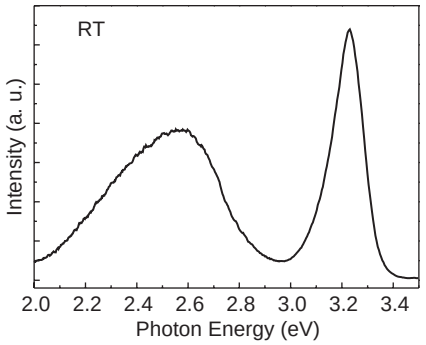

Fig. 5. The room temperature PL spectrum of the ZnO nanorods.

aforementioned. Shown in Fig. 5 is a near-band edge PL spectrum of ZnO nanorods measured at 6 K. Several sharp peaks observed in the range of 3.0–3.45 eV were attributed to the exciton-related recombination. The inset in Fig. 6 shows the wide range PL spectrum of ZnO nanorods. The features of the PL spectrum can be also classified into two categories: near band-edge emission and deep-level emission, which is relatively weak. The near band edge emission of the ZnO nanorods is dominated by the bound exciton peak at 3.370 eV, similar to the previous report [20], due to recombination of excitons bound to donors or acceptors, as depicted in Fig. 6. Since the as-grown ZnO thin film is generally n-type, the bound exciton peak is most likely related to the excitons bound to the neutral donors (D°X), even though the origin of the donor level remains a controversial issue [21–23]. On the high-energy shoulder of the D°X peak, the free exciton A transition (FXA) is observed at 3.383 eV, representing no evidence of quantum confinement as presented in an earlier report in which the diameter of the wires greatly exceeded 20 nm. A weaker structure at even higher energy represents the FXA ($n = 2$) at 3.425 eV. Generally, in II–VI semiconductors, the binding energies of neutral–donor–exciton complexes are smaller than those of excitons bound to neutral acceptors. Thus, the emission labeled A°X most probably belongs to the acceptor–exciton complexes [24]. On the lower energy side of the exciton peaks, the phonon replicas of both FXA at 3.322 eV and D°X at 3.298 eV are identified with the relative energy shift from the exciton peaks by an LO

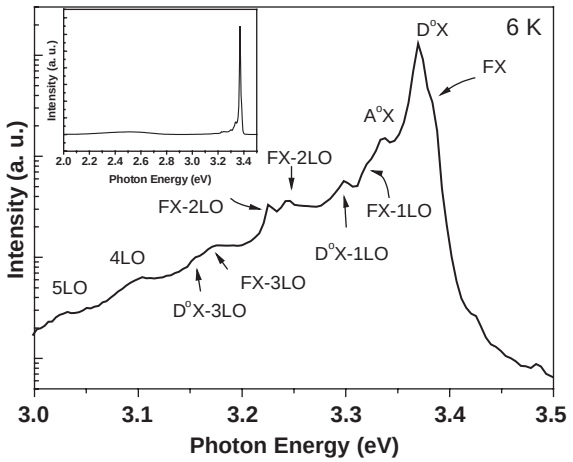

Fig. 6. The near-bandedge emission of the ZnO nanowires measured at 6 K. The inset shows the wide-range PL spectrum.

Table 1
The data of S factor associated with different excitons in ZnO nanorods and epilayer

	S factor associated with D°X	S factor associated with FX
ZnO nanorods	0.044	0.325
ZnO epilayer	0.0136	0.186

phonon energy, respectively. The higher order LO phonon replicas (up to the fifth-order replica of FX) were also observed. In the Franck–Condon model, the coupling strength of the radiative transition to the LO-phonon polarization field is characterized using the Huang–Rhys S-factor [25]. The relative intensity of the nth phonon replicas (I_n) is related to the zero-phonon peak (I_0) by the S-factor as

$$I_n = I_0(S^n e^{-S}/n!), \quad n = 0, 1, 2, \ldots . \tag{1}$$

From the measured spectra, the S-factor associated with D°X is estimated to be approximately 0.044, but the S-factor associated with FXA is around 0.325, which is much higher than that for D°X. It is expected that the coupling of the FXA to the 1LO phonon is stronger than that of D°X due to larger binding energy of FXA exciton, which is closer to the LO phonon energy (72 meV), as compared with D°X exciton [26]. Table 1 shows S-factors of the ZnO nanorods and epitxial layer.

It is found that *S*-factor of the nanorods is more than two times larger than that of the epilayer. It indicates that the strong exciton–phonon interaction in nanorods and thus reducing structure size seems to enhance the probability of exciton–phonon scattering.

4. Conclusions

We have demonstrated the possibility of selective growth of ZnO nanorods on a low temperature grown ZnO buffer layer. The vapor–solid mechanism is responsible for this selective growth of the ZnO nanorods. Although no apparent quantum confinement was observed in these samples from the PL spectra, both of strong edge-emission and phonon-assisted exciton emission in nanorods from low temperature PL spectrum shows good crystalline quality of the grown samples. This low temperature growth technique not only provides a convenient way to grow 1D-ZnO nanostructures in large-area but also opens up an opportunity for fabricating ZnO nanorod-based devices on various low temperature endurance substrates.

Acknowledgements

The authors would like to thank the National Science Council (NSC) and the Ministry of Education of the Republic of China for financially supporting this research under Contract No. NSC 91-2112-M009-016 and 89-E-FA06-AB. And Mr. Hsu gratefully thanks NSC for providing a fellowship.

References

[1] X.F. Duan, Y. Huang, R. Agarwal, C.M. Lieber, Nature 421 (2003) 241.
[2] X.F. Duan, Y. Huang, Y. Cui, J.F. Wang, C.M. Lieber, Nature 409 (2001) 66.
[3] J.F. Wang, M.S. Gudiksen, X.F. Duan, Y. Cui, C.M. Lieber, Science 293 (2001) 1455.
[4] W.S. Shi, Y.F. Zheng, N. Wang, C.S. Lee, S.T. Lee, Appl. Phys. Lett. 78 (2001) 3319.
[5] W.S. Shi, Y.F. Zheng, N. Wang, C.S. Lee, S.T. Lee, J. Vac. Sci. Technol. B 19 (2001) 1115.
[6] M.H. Huang, S. Mao, H. Feick, H.Q. Yan, Y.Y. Wu, H. Kind, E. Weber, R. Russo, P.D. Yang, Science 292 (2001) 1897.
[7] M.H. Huang, Y.Y. Wu, H. Feick, N. Tran, E. Weber, P.D. Yang, Adv. Mater. 13 (2001) 113.
[8] Y.W. Wang, L.D. Zhang, G.Z. Wang, X.S. Peng, Z.Q. Chu, C.H. Liang, J. Crystal Growth 234 (2002) 171.
[9] B.D. Yao, Y.F. Chan, N. Wang, Appl. Phys. Lett. 81 (2002) 757.
[10] C.K. Xu, G.D. Xu, Y.K. Liu, G.H. Wang, Solid State Commun. 122 (2002) 175.
[11] Y. Li, G.W. Meng, L.D. Zhang, F. Phillipp, Appl. Phys. Lett. 76 (2000) 2011.
[12] W.I. Park, D.H. Kim, S.W. Jung, G.C. Yi, Appl. Phys. Lett. 80 (2002) 4232.
[13] Y. Dai, Y. Zhang, Y.Q. Bai, Z.L. Wang, Chem Phys. Lett. 375 (2003) 96.
[14] R.S. Wagner, W.C. Ellis, Appl. Phys. Lett. 4 (1964) 89.
[15] Z.W. Pan, Z.R. Dai, Z.L. Wang, Science 291 (2001) 1947.
[16] J.Q. Hu, Q. Li, N.B. Wong, C.S. Lee, S.T. Lee, Chem. Mater. 14 (2002) 1216.
[17] P. Yang, C.M. Lieber, J. Mater. Res. 12 (1997) 2981.
[18] W.-J. Li, E.-W. Shi, W.-Z. Zhong, Z.-W. Yin, J. Crystal Growth 203 (1999) 186.
[19] J.K. Jian, X.L. Chen, W.J. Wang, L. Dai, Y.P. Xu, Appl. Phys. A 76 (2003) 291.
[20] W.I. Park, Y.H. Jun, S.W. Jung, G.C. Yi, Appl. Phys. Lett. 82 (2003) 964.
[21] D.C. Look, J.W. Hemsky, J.R. Sizelove, Phys. Rev. Lett. 82 (1999) 2552.
[22] C.G. Van de Walle, Phys. Rev. Lett. 85 (2000) 1012.
[23] S.F.J. Cox, E.A. Davis, S.P. Cottrell, P.J.C. King, J.S. Lord, J.M. Gil, H.V. Alberto, R.C. Vilão, J. Piroto Duarte, N. Ayres de Campos, A. Weidinger, R.L. Lichti, S.J.C. Irvine, Phys. Rev. Lett. 82 (1999) 2552.
[24] C.F. Klingshirn, Semiconductor Optics, Springer, Berlin, Heidelberg, 1994.
[25] K. Huang, A. Rhys, Proc. Roy. Soc. London A 204 (1950) 406.
[26] B. Di Bartolo, R. Powell, Phonon and Resonance in Solids, Wiley, New York, 1990.